Int J Fract (2022) 234:177–193
https://doi.org/10.1007/s10704-021-00563-6

ORIGINAL PAPER

# Characterizations of material constraint effect for creep crack in center weldment under biaxial loading

**Yanwei Dai · Fei Qin · Yinghua Liu · Filippo Berto · Haofeng Chen**

Received: 10 February 2021 / Accepted: 24 June 2021 / Published online: 12 July 2021


**Abstract** Material mismatch effect on the cracking behavior is an important topic for those welding structures. Characterization of the material constraint effect based on rigorously asymptotic solution is studied in this paper. Based on decomposition of the second order term, the constraint effect characterization parameter is decomposed as material constraint parameter and geometry constraint parameter. In general, the total constraint level for crack tip under undermatch condition is higher than overmatch condition. The specimen with positive biaxiality could lead to a higher constraint level compared with that of negative biaxiality. Geometry constraint effect and material constraint effect could not be separated independently from rigorously asymptotic solution for those cases with positive biaxiality. For a crack tip field under non-positive biaxiality, the material constraint effect can be characterized independently although it is approximate. For these conditions, the proposed material constraint effect and geometry constraint effected characterized are approximately independent on material mismatch factor, crack depth ratio and stress biaxiality. An empirical formula has been presented to characterize the geometry constraint effect and material constraint effect for the crack tip in the weldment under biaxial loading, which has been verified with fine accuracy.

**Keywords** Constraint effect · Material constraint · Mismatch factor · Biaxial loading · Higher order asymptotic solution

Y. Dai (✉) · F. Qin
Institute of Electronics Packaging Technology and Reliability, Faculty of Materials and Manufactruing, Beijing University of Technology, Beijing 100124, China
e-mail: ywdai@bjut.edu.cn

Y. Dai · F. Qin
Beijing Key Laboratory of Advanced Manufacturing Technology, Beijing University of Technology, Beijing 100124, China

Y. Liu
Department of Engineering Mechanics, AML, Tsinghua University, Beijing 100084, China

F. Berto
Department of Engineering Design and Materials, NTNU, Richard Birkelands vei 2b, 7491 Trondheim, Norway

H. Chen
Department of Mechanical & Aerospace Engineering, University of Strathclyde, Glasgow G1 1XJ, UK

## 1 Introduction

Welding components are commonly found in mechanical fields such as pressure vessels and pipelines in various engineering backgrounds. Evaluations of cracked weldment are important topics in this area as Type IV cracking or cracking in heat affected zone

(HAZ) are found commonly in weldment (Wang et al. 2020; Sharifi et al. 2018; Mehmanparast et al. 2020; Wang et al. 2021). Creeping occurs for those weldment components under high temperatures, which can lead to significant creep damage (Yang and Xuan 2018). For crack in creep solids, it is generally denoted as the creep crack to distinguish the cracking in creeping solids and traditionally cracking in elastoplastic solids. For those flawed structures and materials under higher temperature, accurate characterizations and evaluations of crack tip field for creeping solids become a great challenge for industrial and scientific fields, and they are also one of the most important topics in recent years (Saber et al. 2016; Xu et al. 2017a; Xu et al. 2017b; Dai et al. 2017; Dai et al. 2020a; Chao et al. 2001; Wang et al. 2010; Tan et al. 2014; Ma et al. 2016; Cui and Guo 2020; Guo et al. 2018).

The critical challenge on quantifying the stress field of crack tip in those welded components is that the crack tip field can be influenced by many factors such as material mismatch (Kumar et al. 2014), weldment geometry (Zhou et al. 2014), residual stress (Ren et al. 2009) and loading state, e.g., biaxial loading (Wang 2012; Shlyannikov et al. 2011; Shlyannikov et al. 2014; Wang et al. 2014). Those factors can lead to the variations of microstructure (Kulkarni et al. 2020), stress level (Han et al. 2015), fracture toughness (Hemer et al. 2020) as well as crack growth rate (Krishnan et al. 2018; Alves et al. 2020; Velu 2018) for the weldment, among which fracture toughness is an crucial fracture parameter to be determined as it can affect the border of failure assessment diagram which has been widely used as the evaluation tool by the industrial field (Dai et al. 2020a). Note that the fracture toughness is always related to the so-called "constraint effect."

In order to characterize the constraint effect of creep crack, many constraint effect characterization theories have been presented. The early work given by Nguyen et al. (2000) showed the perspective of the asymptotic theory under creeping condition. Chao and coworkers (2001) extended the three order term asymptotic solution to the crack tip field in creeping solids smoothly. Budden and Ainsworth (1999) extended the $Q$-parameter to modify the time-dependent failure assessment diagram for creeping solids. Nikbin (2004) adopted the $Q$-parameter to correlate the creep crack growth rate. Zhao et al. (2015) also performed the creep crack growth rate modification considering constraint effect based on $Q^*$-parameter. Wang et al. (2010) proposed the $R$-parameter to characterize the constraint effect transfer between different specimens with different levels. A series of studies (Tan et al. 2014; Ma et al. 2016) based on the work of Wang et al. (2010) have validated the applicability of the theory. Guo and colleagues (2018, 2020) took out-of-plane factor, $T_z$, into account, and proposed the constraint characterization method for three dimensional creep crack front. Recently, the works given by Dai et al. (2017; 2019; 2020b; 2021) reported the higher order term solutions for crack under mode II and sharp V-notch in creeping solids. Wu et al. (2020) recently presented an insight on the engineering application of $Q^*$-parameter.

In fact, those aforementioned constraint parameters are originally proposed for homogeneous materials without considering material mismatch or biaxial loading. To overcome this shortage, some investigations have been presented to study the relation between constraint effect and material mismatch as well as biaxial loading.

The studies carried out by Lei (2004), Wang et al. (2014) and recently Dai et al. (2020b) showed that the fracture parameter $J$-integral and $C^*$-integral were both affected by the biaxial loading state. Henry and Luxmoore (1997) made an investigation on the biaxial effect on the $Q$-value and stress tiraxiality. The further discussion on creep crack growth prediction considering stress triaxility is presented by Alang and Nikbin (2018). A discussion on the biaxial loading for surface crack was given by Wang (2012), where the solutions were analyzed based on the constraint parameter $Q$ in elastoplastic solids. Also for elastoplastic solids, investigations of biaxial effect on the crack tip field as well as crack growth are presented by Shlyannikov and coauthors (2011, 2014). O'Dowd et al. (1999) also performed a study on the biaxial effect on the center cracked plate. According to Shlyannikov et al. (2009), the crack tip field was controlled by biaxial ratio through higher order constraint parameters regardless of creep or elastoplastic solids.

Aware of the material mismatch effect in the weldment, two parameter methods were presented to characterize the interface crack in elastoplastic plate by Zhang and coauthors (1996, 1997) where difference schemes for stress field between reference stress field and mismatched stress field were proposed.

Burstow et al. (1995, 1998) proposed a relation between constraint parameter $Q$ and the mismatch factor under elastoplastic condition, which showed a clear demonstration of the constraint effect related with mismatch factor. Lately, Kumar et al. (2014) proposed a model to predict the stress component of welded center crack based on correlation of constraint parameter $Q$. Recently, Fan et al. (2016) also presented a unified parameter on predicting the fracture toughness of weldment considering out-of-plane and in-plane effects. More recent works by Duan and Zhang (2020) and Zhang et al. (2020) also show evidence of the increasing interest in studying the so-called "material constraint effect". Material constraint effect here can be understood as the constraint variations of a crack tip caused by material mismatching. Inspired by the material constraint effect studied in elastoplastic condition, the material mismatch effect on the creep crack tip field is reported by Dai et al. (2016) through $M^*$-parameter by analysis of the discrepancy of creep crack tip field under small scale creep. A more recent work can be found in Jiang et al. (2020) for creeping braze joint.

Although some attempts have been made to investigate the material constraint effect, nearly all the known characterization parameters regarding to material constraint effect are empirical or approximate from the perspective of rigorously asymptotic solution. The evidence shown in elastoplastic condition (Burstow et al. 1998) indicates that the constraint effect caused by material mismatch was dependent on the mismatch factor, the weld size and the level of stress intensity characterized by the leading term such as $J$-integral. Then the following problems come up naturally if we limit the condition under creeping condition. Can material constraint effect be characterized independently under creeping conditions based on rigorously higher order asymptotic solutions? What is the relation between constraint level caused by the loading state and the constraint effect caused by material mismatch? Is material constraint effect only dependent on the material mismatch factor?

In order to answer the aforementioned questions, a crack model in the weldment center under biaxial loading with creeping condition is studied in this paper. The main objective of the current paper is to make a thorough study on the characterizations of constraint effect caused by material mismatch, which allows for consideration of the influence of biaxial loading and material mismatch equally. The possibility of the material constraint effect characterization based on higher order term solutions is discussed. Towards this objective, the organization of this paper is given as below. The theoretical foundation is presented in Sect. 2 where the higher order term solutions are revisited. The decomposition of higher order term is introduced in which the geometry constraint effect and material constraint effect are defined. The numerical procedures are illustrated in Sect. 3. The results and discussion are given in Sect. 4. The conclusions are drawn in the last Section.

## 2 Problem statement and theoretical foundation

The typical power-law creep constitutive equation is given as:

$$\dot{\varepsilon}_{ij} = \frac{1+v}{E}\dot{S}_{ij} + \frac{1-2v}{3E}\dot{\sigma}_{kk}\delta_{ij} + \frac{3}{2}\dot{\varepsilon}_0\left(\frac{\sigma_e}{\sigma_0}\right)^{n-1}\frac{S_{ij}}{\sigma_0} \quad (1)$$

$$S_{ij} = \sigma_{ij} - \sigma_{kk}\delta_{ij}/3 \quad (2)$$

$$\sigma_e^2 = \frac{3}{2}S_{ij}S_{ij} \quad (3)$$

where $\dot{\varepsilon}_{ij}$, $\dot{\sigma}_{kk}$, $S_{ij}$, $\dot{\varepsilon}_0$, $\sigma_0$, $\sigma_e$, $E$ and $n$ are strain rate, stress rate, deviatoric stress, reference strain rate, nominal yielding stress, Mises equivalent stress, Young's modulus and creep exponent, respectively. The creep coefficient $C$ is identical to $\dot{\varepsilon}_0/\sigma_0^n$. The quantities with dots represent the differential of creep time. If the elastic strain is much less than the creep strain, Eq. (1) can be simplified as following with the uniaxial stress state.

$$\begin{cases} \dot{\varepsilon}_b = C_b\sigma^{n_b} \\ \dot{\varepsilon}_W = C_W\sigma^{n_W} \end{cases} \quad (4)$$

in which $C_\mathrm{b}$, $C_\mathrm{W}$, $n_\mathrm{b}$ and $n_\mathrm{W}$ are the creep coefficients and creep exponents of the base metal and weld metal, respectively. $\sigma$ and $\dot{\varepsilon}$ are the stress and strain rate, respectively. The subscripts "$b$" and "$W$" represent the base metal and weld metal shown in Fig. 1, respectively.

In order to characterize the mismatch effect of materials, mismatch factor is defined to characterize the mismatch effect. Referred to the strength mismatch of two materials, the mismatch in creep

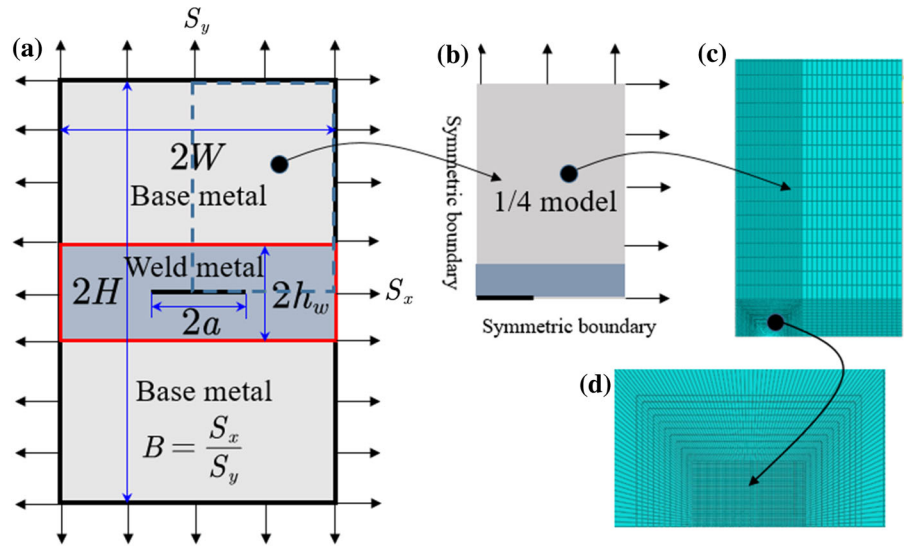


**Fig. 1** Model of a crack in center of weldment under biaxial loading: **a** geometry model, **b** 1/4 model, **c** FE mesh and **d** crack tip mesh

property between base metal and weld metal can be defined as (Xuan et al. 2004)

$$m = \left(\frac{C_b}{C_W}\right)^{1/n} \tag{5}$$

The limitation of Eq. (5) is that the creep exponents of base metal and weld metal are assumed to be the same. If mismatch factor "$m$" is greater than 1, it represents the overmatch. In case of "$m$" is less than 1, it means the undermatch condition.

For crack tip field in homogeneous material, the constraint effect of crack tip field is described by a higher order term. Herein, the three-term asymptotic solution for creep crack-tip field developed by Chao et al. (2001) was adopted to perform the analysis. The form of the three ordered term asymptotic solution for creep crack under mode I loading is given as following:

$$\frac{\sigma_{ij}(r,\theta;t)}{\sigma_0} = A_1(t)\left[\bar{r}^{s_1}\tilde{\sigma}_{ij}^{(1)}(\theta) + A_2(t)\bar{r}^{s_2}\tilde{\sigma}_{ij}^{(2)}(\theta) + A_3(t)\bar{r}^{s_3}\tilde{\sigma}_{ij}^{(3)}(\theta)\right] \tag{6}$$

$$A_1(t) = \left(\frac{C(t)}{\sigma_0\dot{\varepsilon}_0 I_n L}\right)^{-s_1} \tag{7}$$

$$s_1 = -\frac{1}{n+1} \tag{8}$$

where $A_1(t)$, $A_2(t)$ and $A_3(t)$ are the terms of different orders, and there follows $A_3(t) = A_2^2(t)$. $s_1$, $s_2$ and $s_3$ are the stress exponents of different orders, respectively. $\tilde{\sigma}_{ij}^{(k)}(\theta)$ is the angular distribution function for k-th order terms. The dimensionless integration constants $I_n$ are only related to the creep exponent $n$ and independent of other material property and the applied loads. $\bar{r} = r/L$ and $L$ is a characteristic length parameter which can be taken as the crack length $a$, the specimen width $W$ and so on. $C(t)$ is the creep fracture parameter $C(t)$-integral which is defined as below (Landes and Begley 1976):

$$C(t) = \int_{\Gamma\to 0}\left(W^* \mathrm{d}y - T_i\left(\frac{\partial \dot{u}_i}{\partial x}\right)\mathrm{d}s\right) \tag{9}$$

where $\Gamma$ is a counterclockwise integral path of crack tip, and $T_i$, $\dot{u}_i$, $\mathrm{d}y$ and $\mathrm{d}s$, are the traction vector of integral path, the displacement rate, the increments of $y$-direction and integral path, respectively. When the creep crack is at extensive creep stage, the stress distribution around the crack tip is constant and the steady creep fracture parameter $C^*$ is used to characterize the intensity of the crack-tip fields. The characteristic time $t_T$ for transition from small-scale creep to extensive creep is estimated and given as (Riedel 1990)

$$t_T = \frac{K_I^2(1-\nu^2)}{(n+1)EC^*} \tag{10}$$

The transition time $t_T$ are related to the applied load, crack length and the elastic and creep properties of materials.

To calculate the constraint level of different factors, here we assume that the second order term, $A_2(t)$, of Eq. (6) is composed separately by $A_{2\mathrm{I}}(t)$ and $A_{2\mathrm{II}}(t)$, i.e.

$$A_2(t) = A_{2\mathrm{I}}(t) + A_{2\mathrm{II}}(t) \tag{11}$$

where $A_{2\mathrm{I}}(t)$ and $A_{2\mathrm{II}}(t)$ are constraint parameters to characterize the constraint effect caused by biaxial loading, crack depth, and the constraint effect caused by material mismatch. Thus, the stress field described by Eq. (6) is written as below:

$$\frac{\sigma_{ij}(r,\theta;t)}{\sigma_0} = A_1(t)\left[\vec{r}^{s_1}\tilde{\sigma}_{ij}^{(1)}(\theta) + (A_{2\mathrm{I}}(t)+A_{2\mathrm{II}}(t))\vec{r}^{s_2}\tilde{\sigma}_{ij}^{(2)}(\theta) + (A_{2\mathrm{I}}(t)+A_{2\mathrm{II}}(t))^2\vec{r}^{s_3}\tilde{\sigma}_{ij}^{(3)}(\theta)\right] \tag{12}$$

The introduction of $A_{2\mathrm{I}}(t)$ and $A_{2\mathrm{II}}(t)$ will lead to some complications in determining them. To overcome this problem, a standard reference stress field will be set up. On determination of the second order terms such as $A_{2\mathrm{I}}^*$ and $A_{2\mathrm{II}}^*$, we should firstly retrospect to the determination of $A_2(t)$. The determination of $A_2(t)$ can refer to the point match method given by Chao et al. (2001). The standard reference stress field is obtained under the condition that the stress field is in homogeneous material ($m = 1$) with a fixed biaxial loading ratio $B$. If the biaxial ratio $B$ is fixed, then the $A_{2\mathrm{II}}(t)$ will be obtained. Similarly, if one wants to obtain $A_{2\mathrm{I}}(t)$, the mismatch factor should be unchanged. With this decoupling method and in combination with the point match method, $A_{2\mathrm{I}}(t)$ and $A_{2\mathrm{II}}(t)$ can be solved easily. The symbol "*" is added in the superscript, i.e. $A_{2\mathrm{I}}^*$, $A_{2\mathrm{II}}^*$ and $A_1^*$, to denote the values of those terms in Eq. (12) under extensive creep.

## 3 Numerical procedures

With the theoretical background given in Sect. 2, a mismatched two-dimensional center-cracked weldment plate is established in Fig. 1. The typical finite element mesh for the model is also given in Fig. 1. The crack is located in the center of the weld metal. The plate has the dimensions with fixed height-width ratio $H/W = 2$. The slenderness of the weldment $(W - a)/h_{\mathrm{W}}$ is fixed as 4 during the computation of this paper. To investigate the influence of crack depth on the creep crack-tip stress field, three types of crack depth ratios are selected, i.e. $a/W = 0.2$, 0.4 and 0.6, where $W$ is 100 mm.

The plate is subjected to biaxial loading, as depicted in Fig. 1, the stress biaxiality is defined by biaxial ratio factor $B$, i.e.

$$B = S_x/S_y \tag{13}$$

where $S_y$ is the remote uniform pressure loading perpendicular to the crack and $S_x$ is the remote uniform pressure loading parallel to the crack. Note that the case $B = 0$ corresponds to uniaxial tension, and the case $B = 1$ represents the equibiaxial loading condition. In present work, to study the impact of biaxial loading on the crack constraint level, $S_y$ is constant, i.e. $S_y = 50$ MPa, and the value of $B$ ranges from -1 to 1 by changing the value and sign of $S_x$.

Finite element analyses are performed on commercial software ABAQUS. A quarter of the plate, due to the symmetry in both geometry and loading, is modelled with plane strain condition. The typical finite element meshes are illustrated in Fig. 1c. The element type used here is four-node linear plane strain element (CPE4H). The mesh consists of 8925 elements and the minimum length of the element is 0.0067 mm to ensure the calculation accuracy.

For the convenience of analysis and calculation, it is assumed that the elastic properties of weld metal and base metal are identical, i.e., the nominal stress $\sigma_0$, Young's modulus $E$ and Poisson ratio $v$ for the weld metal and base metal are taken as 180 MPa, 125,000 MPa and 0.3, respectively. These materials are close to the 1/2CrMoV steel for base material and 2.25Cr1Mo steel for weld material, which have been used widely in high temperature pressure vessels (Han et al. 2015). It implies that there is no elastic mismatch discussed in this paper so as to make the investigation be focused on creeping mismatch. The mismatch factor "$m$" varies between 0.58 and 2.00, and the detail mismatch factors defined with different material constants are given in Table 1.

**Table 1** Material constants used in the computation

| $C_b$ | $C_W$ | $m$ | $n$ |
|---|---|---|---|
| 3.20E-11 | 1.60E-10 | 0.58 | 3 |
| 3.20E-11 | 1.00E-10 | 0.68 | 3 |
| 3.20E-11 | 8.00E-11 | 0.74 | 3 |
| 3.20E-11 | 6.40E-11 | 0.79 | 3 |
| 3.20E-11 | 3.20E-11 | 1 | 3 |
| 3.20E-11 | 1.60E-11 | 1.26 | 3 |
| 3.20E-11 | 8.00E-12 | 1.59 | 3 |
| 3.20E-11 | 4.00E-12 | 2.00 | 3 |

## 4 Results and discussions

### 4.1 Variations of $C(t)$-integral

The fracture parameter $C(t)$-integral at steady-creep stage is the typical $C^*$-integral which is independent of the integral contours. Figure 2 is presented to state the effect of biaxial loading and material mismatch on $C^*$-integral for the center cracked weldment plate with $a/W = 0.2$. Note that $C^*$-integral in Fig. 2 is obtained by taking the average value for $C(t)$-integral of nine contours around the crack tip at steady-creep stage. As it can be seen from Fig. 2, $C(t)$-integral decreases with the increments of mismatch factor $m$ and biaxiality $B$. It can be found that $C(t)$-integral becomes steady if the transition time is greater than $10t_T$.

To present the variations of $C(t)$-integral under extensive creep, $C^*$-integral of different cases with

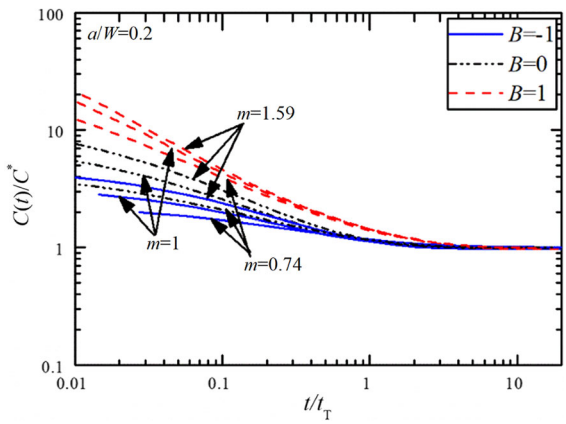


**Fig. 2** Variations of $C(t)/C^*$ with normalized creep time under biaxial loading and various mismatch factors

various mismatch factors and biaxial ratios are extracted directly from the numerical analysis, which are shown in Fig. 3. It can be found that the value of $C^*$-integral decreases with the increase of mismatch factor under the same bixiality regardless of short crack plate and deep crack plate. For a fixed mismatch factor, the biaxial stress effect on $C^*$-integral is also clear. In general, $C^*$-integral heightens with the decrease of the biaxial ratio.

### 4.2 Quantifying the stress field of the crack in weldment

#### *4.2.1 Radial stress distributions*

The radial distributions for $\sigma_{\theta\theta}$ and $\sigma_{rr}$ ahead of the crack-tip ($\theta = 0°$) at the steady-creep stage are presented in Fig. 4 for the welded plate with $a/W = 0.2$, where the stresses are normalized by the nominal stress $\sigma_0$ and the radial distance $r$ is normalized by the half crack length $a$. As shown in Fig. 4, the influence of the material mismatch on the radial stress distributions of $\sigma_{\theta\theta}$ and $\sigma_{rr}$ strongly depends on the biaxial loading. Otherwise, the stress components along the radial direction are affected by the material mismatch significantly. The differences between various stress components rely on the material mismatch and biaxial loading.

For the stress components $\sigma_{\theta\theta}$, the stress distribution is nearly unaffected by the material mismatch if biaxial factor $B = -1$. However, the stress increases rapidly with the material mismatch when the biaxial factor increases from $B = -1$ to $B = 1$. For the stress component $\sigma_{rr}$, the stress distribution is nearly independent on the material mismatch within the finite strain zone $r/a < 0.02$ under $B = -1$. However, it decreases with the mismatch factor if $r/a \geq 0.02$. The stress distribution of $\sigma_{rr}$ increases with the increment of the mismatch factor $\sigma_{rr}$ under $B = 1$.

#### *4.2.2 Angular stress distributions*

Although the radial stress distributions shown in Sect. 4.2.1 present the variations of the stress components with material mismatch factor, a more direct evidence on the effect of material mismatch on crack tip stress field is given in Fig. 5, where the dimensionless angular distributions for stress components $\sigma_{\theta\theta}$, $\sigma_{rr}$ and $\sigma_{r\theta}$ normalized by nominal stress $\sigma_0$ at the

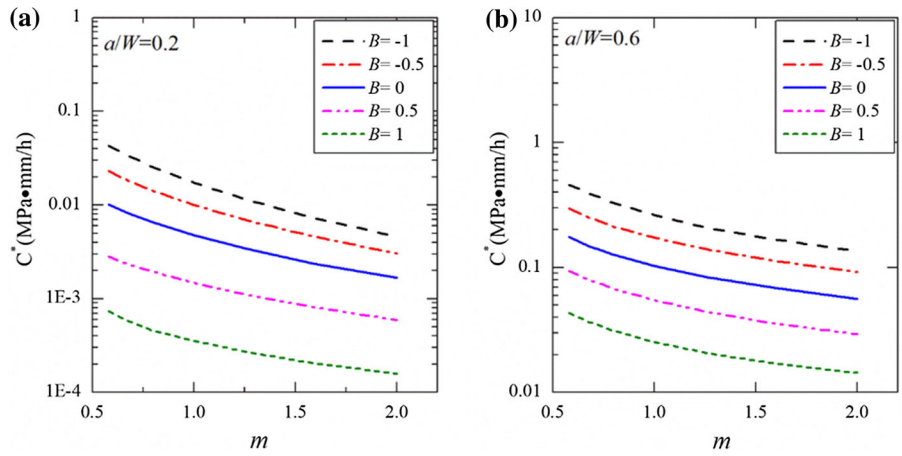


**Fig. 3** Variations of $C^*$-integral with different mismatch factors

position from the crack tip $r/a = 0.083$ at extensive creep $t = 10t_T$ are presented in Fig. 5.

From Fig. 5, the influences of the material mismatch on the angular distribution of the stress components $\sigma_{\theta\theta}$, $\sigma_{rr}$ and $\sigma_{r\theta}$ still depend strongly on the biaxial stress states. For the stress components $\sigma_{\theta\theta}$ and $\sigma_{rr}$ with $B = -1$ shown in Fig. 5a, the general tendency is that the stress components decrease as material mismatch factor increases. For uniaxial loading state shown in Fig. 5b, the stress components with overmatch condition hold the higher stress levels. Similar tendencies can be found in Fig. 5c for the condition of biaxial ratio $B = 1$.

## 4.3 Characterizations of material constraint effect

### *4.3.1 Constraint characterization parameter*

According to the result shown in Sect. 4.2, the crack tip field is assured to be affected by the material mismatch. Based on Eq. (12), the higher order term $A_2(t)$ is divided into $A_{2I}(t)$ and $A_{2II}(t)$ where $A_{2I}(t)$ and $A_{2II}(t)$ are the second order terms to characterize the constraint effect caused by geometry factors and material mismatch. Generally, the geometry factors include the crack depth, specimen sizes and loading states. If extensive creep is approached, $A_2(t)$, $A_{2I}(t)$ and $A_{2II}(t)$ are denoted as $A_2^*$, $A_{2I}^*$ and $A_{2II}^*$, respectively. Based on this treatment, the question that we proposed at the start of this paper will become the verification of dependencies for $A_{2I}(t)$ and $A_{2II}(t)$.

On the determination of $A_2(t)$, the point match method will be adopted. In the present research, the stress components of $\sigma_{\theta\theta}$ at within range $r/a = 0.01 \sim 0.1$ along $\theta = 0^\circ$ and $45^\circ$ are used to determine the value of $A_2(t)$ based on Eq. (6). The parameters adopted in Eq. (6) can be found in the table given by Chao et al. (1997). For example, the stress exponents with $n = 3$ for $s_1$, $s_2$ and $s_3$ are -0.25, $-0.01284$ and 0.22432, respectively. The other parameters such as $I_n$, $\tilde{\sigma}_{\theta\theta}^{(1)}$, $\tilde{\sigma}_{\theta\theta}^{(2)}$ and $\tilde{\sigma}_{\theta\theta}^{(3)}$ can also be found in Chao et al. (1997). It should be pointed out that the material constants such as $\sigma_0$, $\dot{\varepsilon}_0$ and $n$ of the weldment are used as the materials constants adopted in Eq. (6).

The variations of $A_2(t)$ with normalized creep time is shown in Fig. 6 where different values of $A_2(t)$ under various biaxial loading states and material mismatch conditions are presented. It is found that $A_2(t)$ term varies to be a constant if creep time exceeds $10t_T$. It implies that $A_2(t)$ become $A_2^*$ when creep time is more than $10t_T$. Moreover, $A_2(t)$ term is different under various material mismatch factors. The constraint parameter $A_2(t)$ decreases with the increase of mismatch factors. It also represents that overmatch condition possesses the lowest constraint level and undermatch condition holds the higher constraint level. If one holds the crack plate to be a homogeneous material, it is seen that the constraint level is lower for negative biaxial ratio compared with the other conditions.

### *4.3.2 Comparisons of stress fields considering higher order term solution*

With the computed $A_2(t)$ term with the point match method, the comparisons for solutions of stress

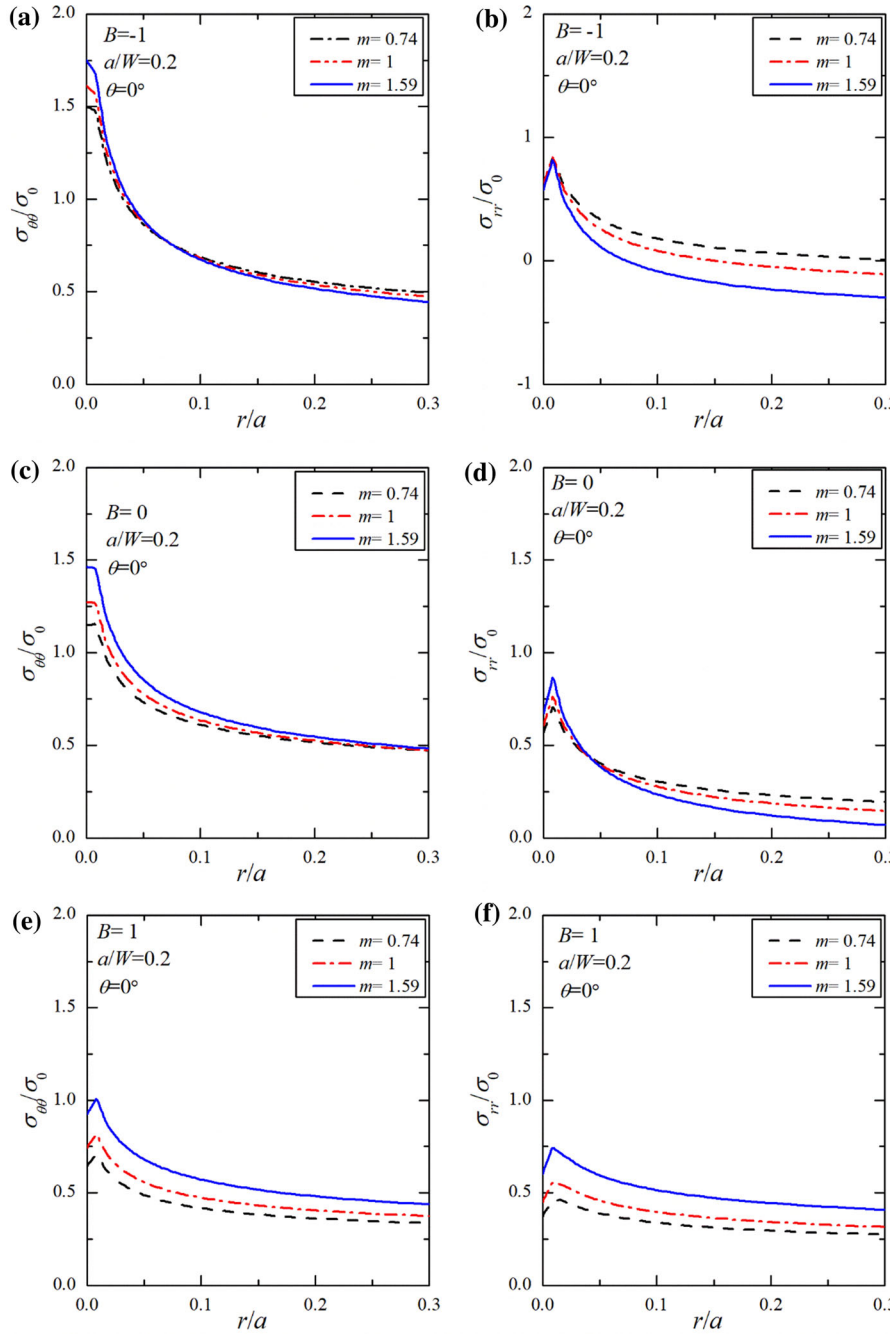


**Fig. 4** Tangential stress and radial tress distributions along $\theta = 0^\circ$ under biaxial loading for $a/W = 0.2$ at $t/t_T = 10$ with different mismatch factors

components in radial direction analyzed with the higher order term solution (HTS), HRR field and finite element method (FEM) are shown in Fig. 7. For Fig. 7a and b, it is found that the HTS solution agrees quite closely with the FE solutions. However, the discrepancy between the HRR solutions and HTS solutions is remarkable under the biaxial ratio $B = -1$ regardless of undermatch condition or overmatch condition. Similar tendencies can be found in Fig. 7c and d. For $B = 1$, the solutions show that the HTS solution, HRR solution and FE solution agree quite closely with each other. The reason could be that it is the equivalent biaxial tension state for $B = 1$. The hydrostatic stress ahead of crack under this condition

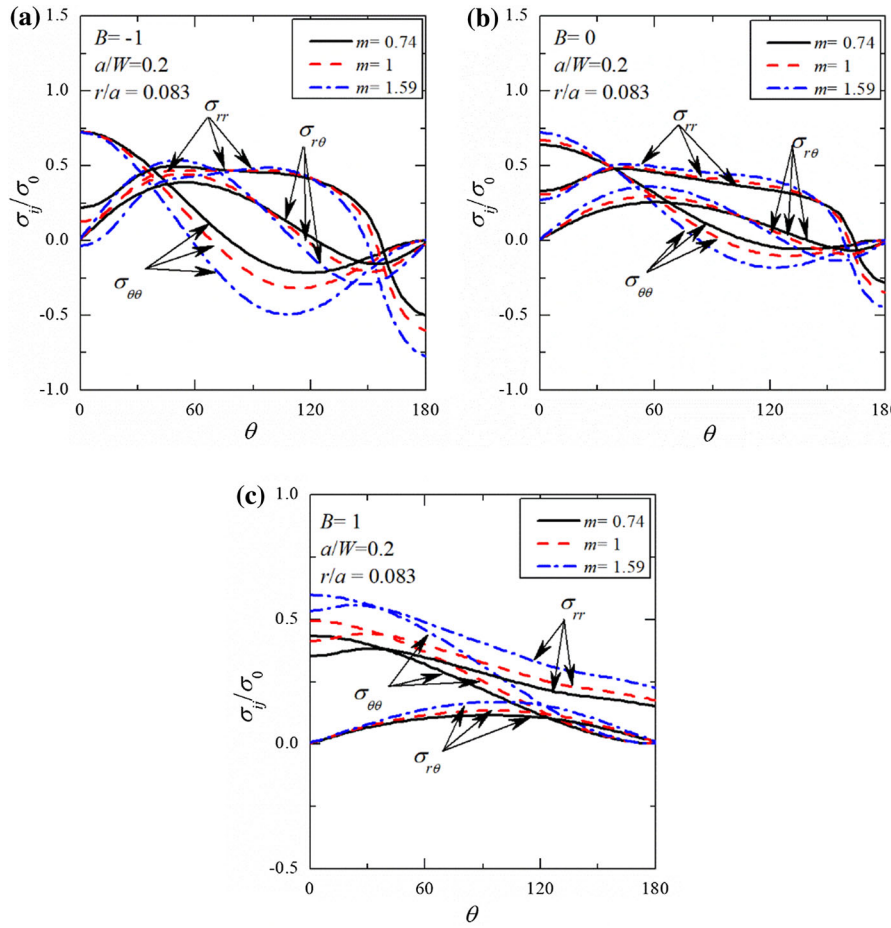


**Fig. 5** Angular distributions of stress components $\sigma_{\theta\theta}$, $\sigma_{rr}$ and $\sigma_{r\theta}$ at $r/a = 0.083$ for $a/W = 0.2$ with $t/t_T = 10$ under various biaxial loadings: **a** $B$ = -1; **b** $B$ = 0; **c** $B$ = 1

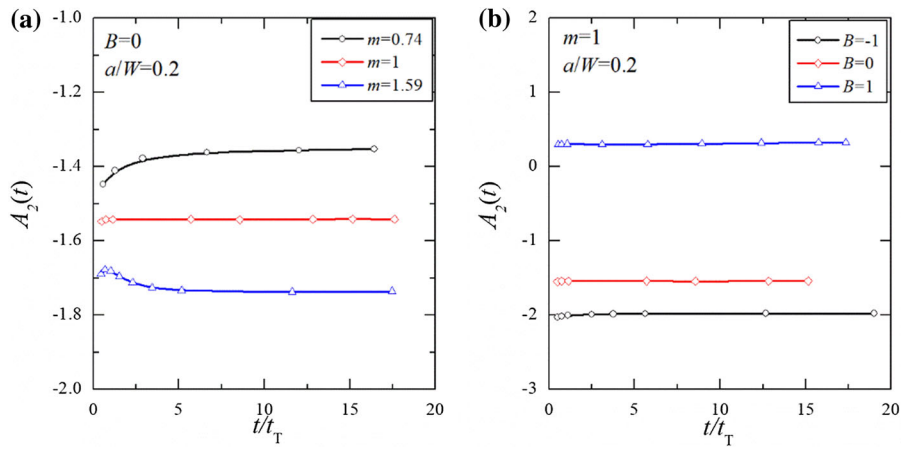


**Fig. 6** Variations of $A_2(t)$ for $a/W = 0.2$ with $t/t_T = 10$ under various **a** mismatch factors and **b** biaxial loadings

is a constant which is not dependent on the material mismatch state.

The comparisons of the stress components in angular direction between HTS solutions, HRR solutions and FE solutions are shown in Fig. 8. It is found that the HTS solutions all agree well with the FE solutions regardless of material mismatch and loading biaxiality. All the solutions shown in Fig. 8

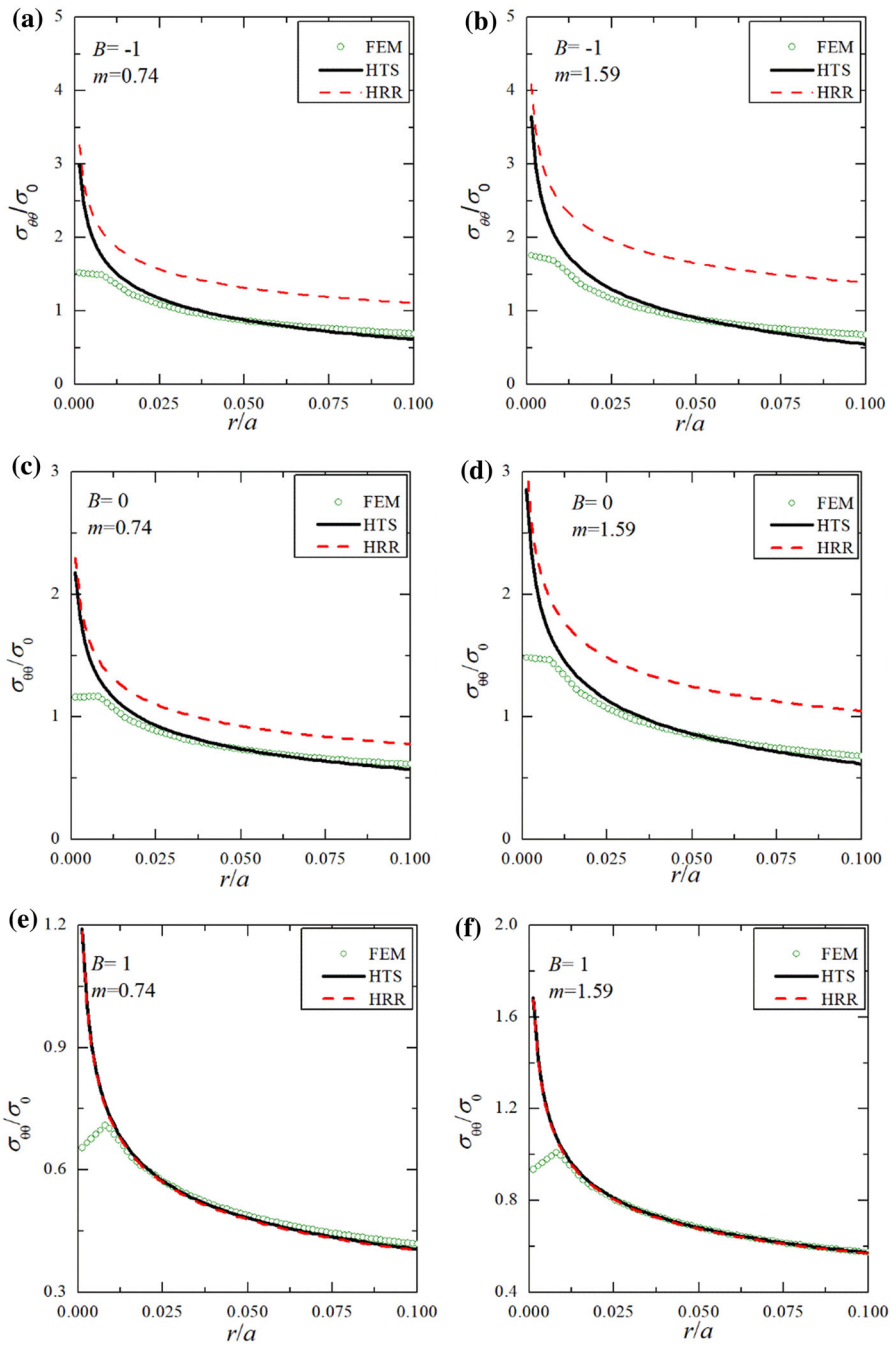


**Fig. 7** Comparisons of HTS, FEM and HRR solutions under various conditions along $\theta = 0^{o}$ for $a/W = 0.2$ at $t = 12t_T$: **a** $B$ = -1, $m$ = 0.74; **b** $B$ = -1, $m$ = 1.59; **c** $B$ = 0, $m$ = 0.74; **d** $B$ = 0, $m$ = 1.59; **e** $B$ = 1, $m$ = 0.74; **f** $B$ = 1, $m$ = 1.59

demonstrates that the method based on the $A_2(t)$-termed solutions enable to predict the stress field correctly. The specific values of $A_2(t)$-term under extensive creep for all the analyzed condition is given in Fig. 9 in which it is found that the constraint parameter $A_2^*$ generally decreases with the increase of mismatch factor. For shallow crack with $a/W = 0.2$, the constraint parameter is generally larger than zero for the condition of $B$ = 1. For other mismatch factors and biaxial ratios, the constraint parameter $A_2^*$ is generally lower than zero. Comparing the constraint level at a fixed mismatch factor, the constraint

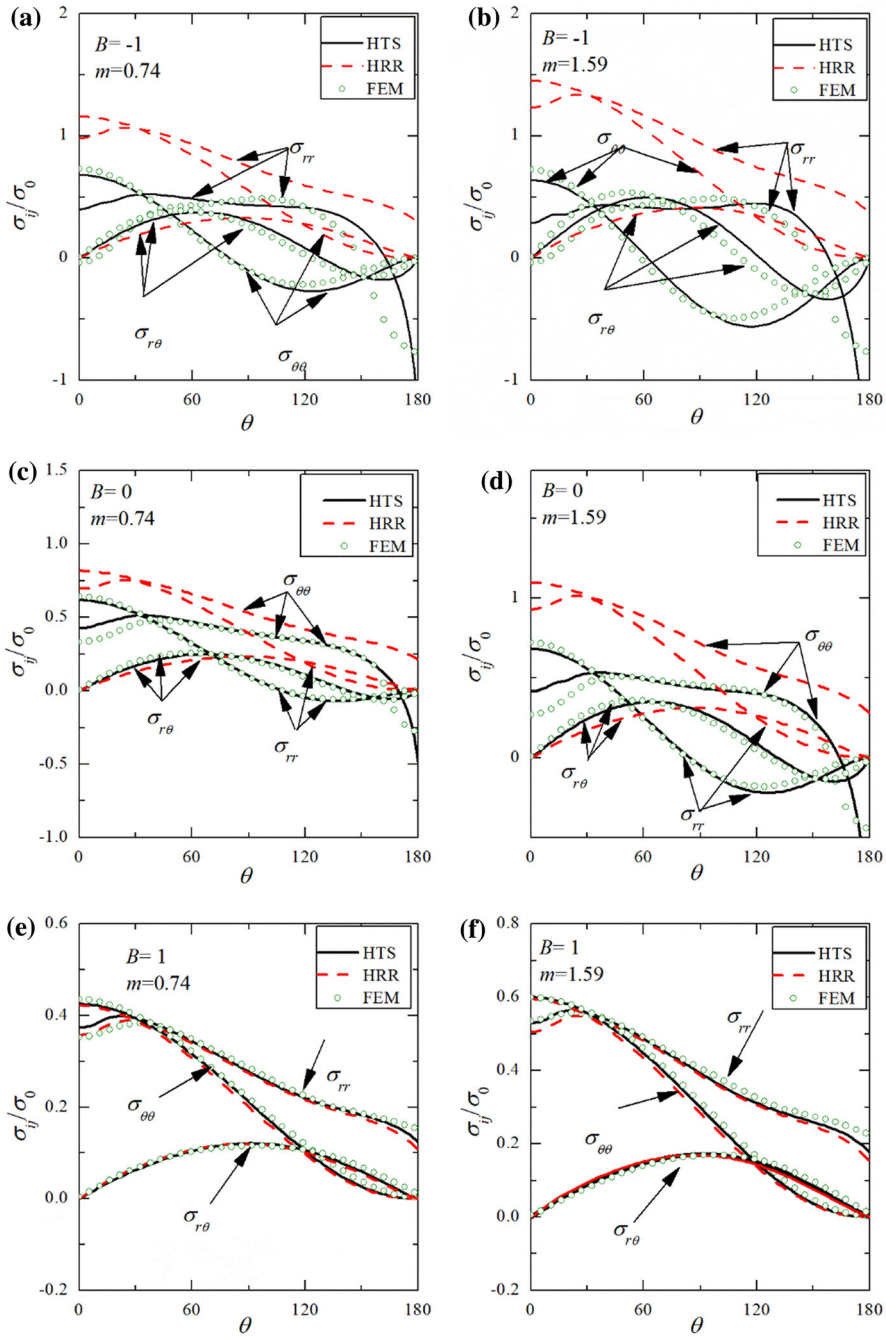


**Fig. 8** Comparisons of stress components in angular direction at $r/a = 0.083$ for $a/W = 0.2$ and $t = 12t_T$: **a** $B = -1$, $m = 0.74$; **b** $B = -1$, $m = 1.59$; **c** $B = 0$, $m = 0.74$; **d** $B = 0$, $m = 1.59$; **e** $B = 1$, $m = 0.74$; **f** $B = 1$, $m = 1.59$

parameter decreases with the decrease of the biaxial ratio.

Figure 10 is presented to see the variations of $A_2^*$ with material mismatch under various crack depths. From Fig. 10, it can be seen that the constraint level is influenced by the material mismatch, crack depth and biaxial state. For condition of $B = -1$, it is found that the crack tip with shallow crack depth holds the the lower constraint level. However, the constraint level for shallow crack is generally larger for the condition of $B = 1$. For uniaxial loading condition, the situations for various crack depths are quite different. As for condition of $a/W = 0.4$, the variation

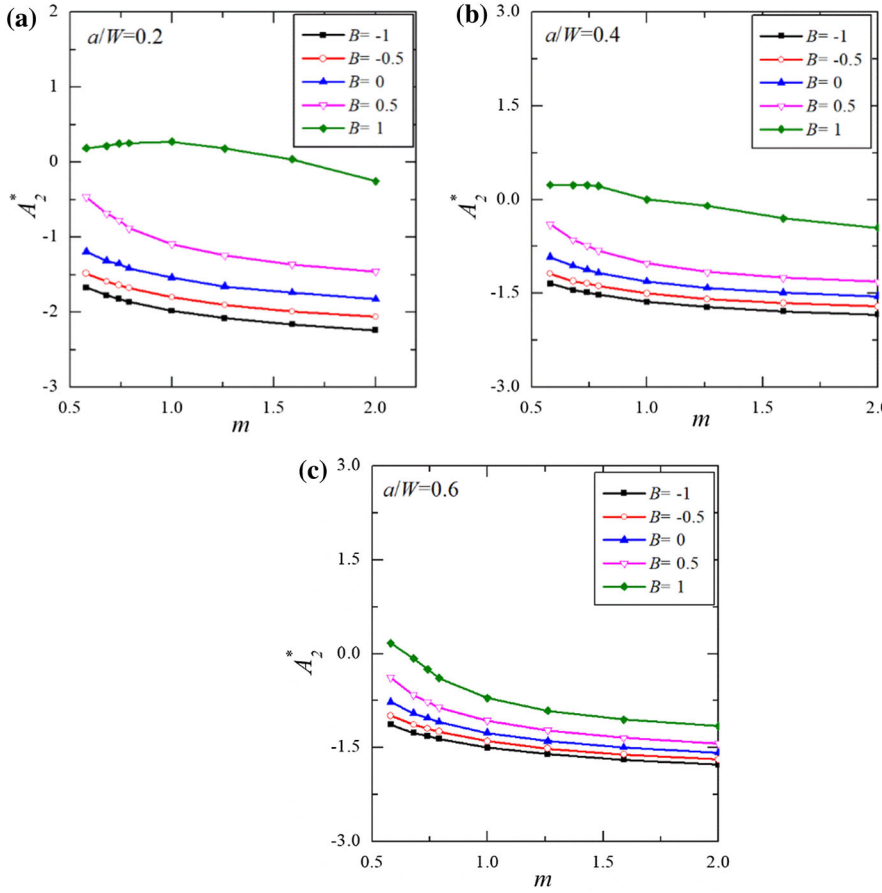


**Fig. 9** Variations of constraint parameter $A_2^*$ with mismatch factor and biaxial loading for different crack geometries **a** $a/W = 0.2$; **b** $a/W = 0.4$; **c** $a/W = 0.6$

tendencies are dependent on the material mismatch under uniaxial loading condition.

#### 4.3.3 *Independent verification of material constraint and geometrical constraint*

According to Eq. (12), here it is firstly assumed that the constraint effect can be separated by generalized geometry constraint parameter $A_{2\mathrm{I}}^*$ and material constraint parameter $A_{2\mathrm{II}}^*$. Based on the computation scheme given in Sect. 2, $A_{2\mathrm{I}}^*$ and $A_{2\mathrm{II}}^*$ can be obtained separately. Note that we assume that $A_{2\mathrm{I}}^*$ is generally dependent on geometry factors including specimen size, loading state and crack depth. Here, two main factors, i.e. crack depth and loading state are selected to make the verification. The variations of $A_{2\mathrm{I}}^*$ with different mismatch factors under various biaxial loading are given in Fig. 11. Two crack depths, i.e. $a/W = 0.2$ and 0.6, are adopted as the presented cases. It is found that the constraint parameter $A_{2\mathrm{I}}^*$ under $B = 0, -0.5$ and $-1.0$ are nearly unchanged with the variations of the mismatch factor. In other words, the constraint level for these conditions can be treated independently on the material mismatch effect. However, the constraint levels of $A_{2\mathrm{I}}^*$ for conditions under $B = 0.5$ and 1.0 varies with the change of mismatch factor $m$, which indicates that $A_{2\mathrm{I}}^*$ is influenced by the mismatch factor.

The evidence that constraint parameter $A_{2\mathrm{I}}^*$ is affected significantly by the biaxial ratio is presented in Fig. 12 where $A_{2\mathrm{I}}^*$ varies with the variations of crack depth and biaxial ratio. From Fig. 12, it is found that the geometry constraint characterized by $A_{2\mathrm{I}}^*$ is higher for the condition with deeper crack length under the condition that the biaxiality is less than zero. Reversely, geometry constraint characterized by $A_{2\mathrm{I}}^*$ is lowest for the condition with deeper crack under the condition that the biaxiality is greater than zero.

Herein, variations of constraint parameter $A_{2\mathrm{II}}^*$ with mismatch factors are presented in Fig. 13. It is seen

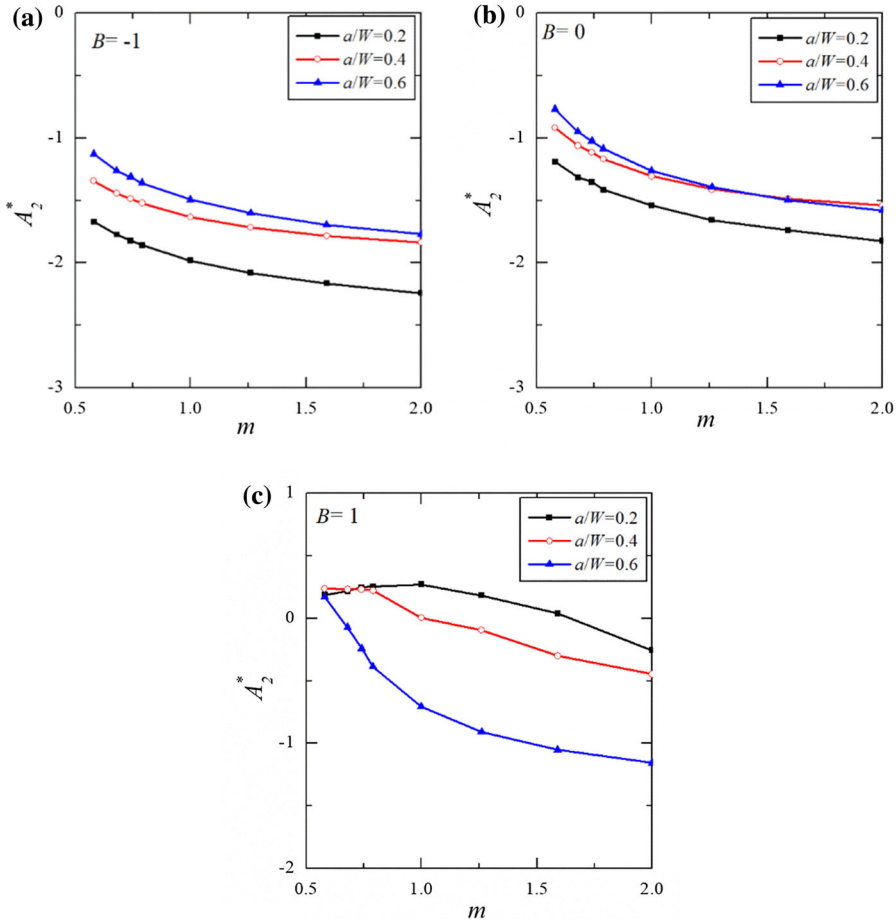


**Fig. 10** Variations of constraint parameter $A_2^*$ with mismatch factor for different crack depths: **a** $B$ = -1; **b** $B$ = 0; **c** $B$ = 1

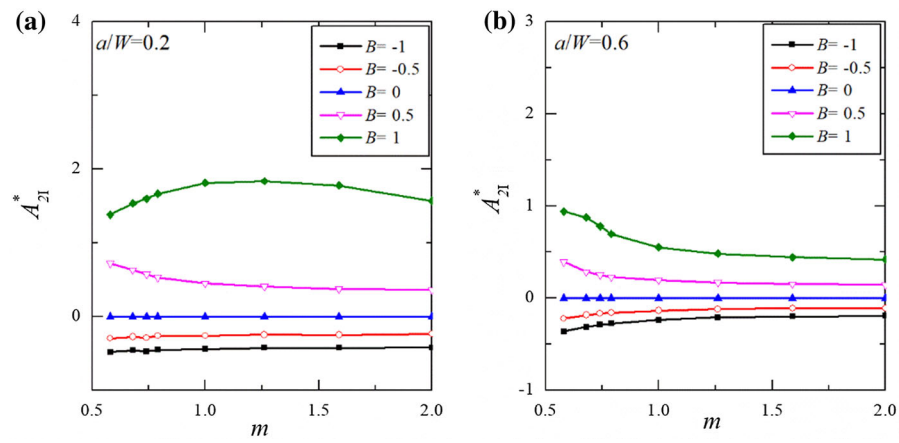


**Fig. 11** Variations of constraint parameter $A_{2I}^*$ with mismatch factor: **a** $a/W$ = 0.2; **b** $a/W$ = 0.6

that $A_{2II}^*$ is not significantly influenced by the material mismatch for cases with $B = -1.0, -0.5$ and 0.0. However, $A_{2II}^*$ is apparently affected by the mismatch factors for cases with $B$ = 1.0 and 0.0. It implies that the constraint effect characterized by $A_{2II}^*$ is not significantly influenced by the biaxial loading state if the biaxial ratios are $-1.0, -0.5$ and 0.0.

Figure 14 is presented to validate the effect of crack depths on the variations of $A_{2II}^*$ for those cases under $B = -1.0$ and $B$ = 0.0. It is found that constraint

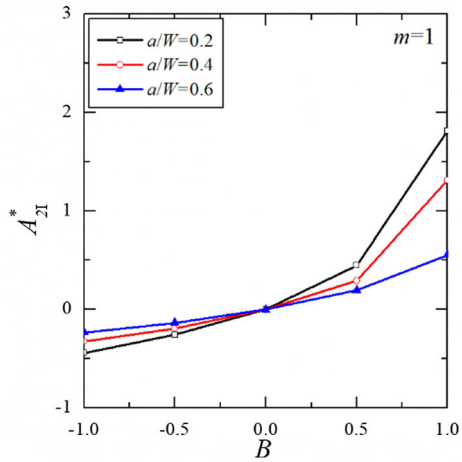


**Fig. 12** Variations of constraint parameter $A^*_{2I}$ with biaxial ratio

parameter $A^*_{2II}$ decreases with the increase of mismatch factor. The values of $A^*_{2II}$ barely change with the variations of crack depth. Hence, it indicates that the material constraint effect is not influenced by the crack depth. In general, the solutions presented in Fig. 13 and Fig. 14 show that the material constraint parameter $A^*_{2II}$ is approximately independent of the crack depth and biaxial stress state for those cases with $B = -1.0, -0.5$ and 0.0. However, $A^*_{2II}$ is dependent on the crack depth and biaxial stress state for those cases with $B = 1.0$ and 0.5.

### 4.4 Discussion

Based on the analyses given in Sect. 4.3, the geometry constraint parameter $A^*_{2I}$ is dependent on the geometry factors only under the condition that the biaxiality is less than or equal to zero. Similarly, the material constraint level $A^*_{2II}$ is only related to the material mismatch under the condition that biaxiality is less than or equal to zero. For positive biaxiality, both geometry constraint parameter $A^*_{2I}$ and material constraint parameter $A^*_{2II}$ are dependent on the stress state, crack depth and material mismatch. In other words, material constraint can be treated independently only under the situation that the biaxiality is not positive.

Thus, the variation of $A^*_{2I}$ with biaxiality under zero can be described with the following fitting formula, where the general geometry constraint parameter $A^*_{2I}$ is a function of stress biaxiality and crack depth ratio.

$$A^*_{2I} = \left[2.31\left(\frac{a}{W}\right)^2 - 2.37\left(\frac{a}{W}\right) + 0.7\right]B^2 + \left[2.83\left(\frac{a}{W}\right)^2 - 3.32\left(\frac{a}{W}\right) + 1.32\right]B - 2.00\left(\frac{a}{W}\right)^2 + 2.25\left(\frac{a}{W}\right) - 1.89 \tag{14}$$

where $a/W$ is the crack depth ratio and $B$ is the stress biaxiality. Note that Eq. (14) is only applicable under the condition that biaxial loading ratio is controlled at least below zero.

Thereafter, the material constraint parameter $A^*_{2II}$ can be also fitted with the following form if biaxial loading ratio is controlled at least below zero:

$$A^*_{2II} = 0.46(m-1)^2 - 0.72(m-1) \tag{15}$$

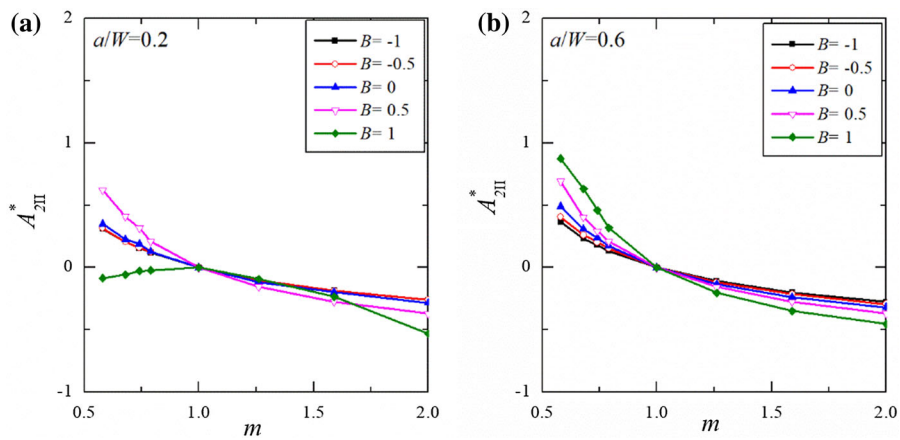


**Fig. 13** Variations of constraint parameter $A^*_{2II}$ with mismatch factor under different crack depths: **a** $a/W = 0.2$; **b** $a/W = 0.6$

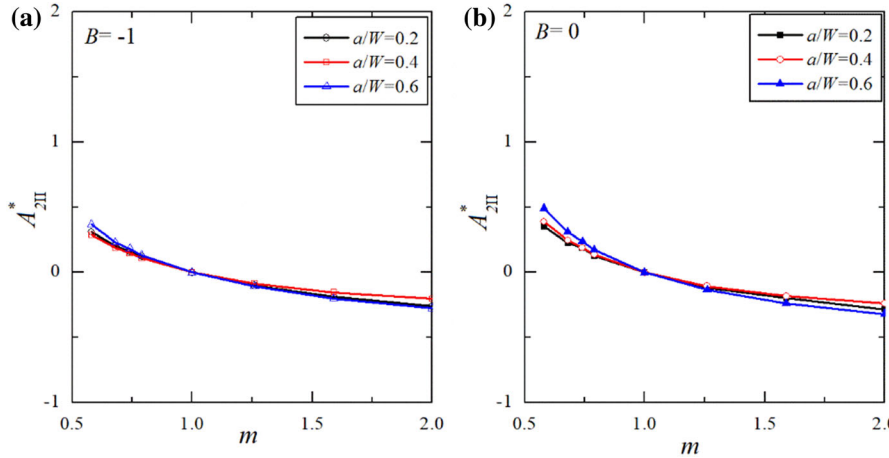


**Fig. 14** Variations of constraint parameter $A^*_{2II}$ with mismatch factor under different crack depths **a** $B$ = -1 **b** $B$ = 0

in which $m$ is the material mismatch factor. It should be noted that there is no limitation on the range limitation of mismatch factors. The only requirement is that the creep exponent of weld metal should be identical to base metal.

In order to validate the fitting solutions given in Eq. (14) and Eq. (15), the tangential stress of a given case under mismatch factor 0.74 is presented in Fig. 15 to show the effectiveness of the given formulae (14) and (15). The case adopted here is arbitrary such that the crack depth, mismatch factor and biaxiality are 0.5, 0.74 and 0. The prediction line shown in Fig. 15 is computed with the predicted $A^*_{2I}$ and $A^*_{2II}$ with formulae (14) and (15). Good agreement is found in Fig. 15 between the predicted stress component and FE solutions, which demonstrates the effectiveness of the method given in this paper. Note that we have noted that there still could be

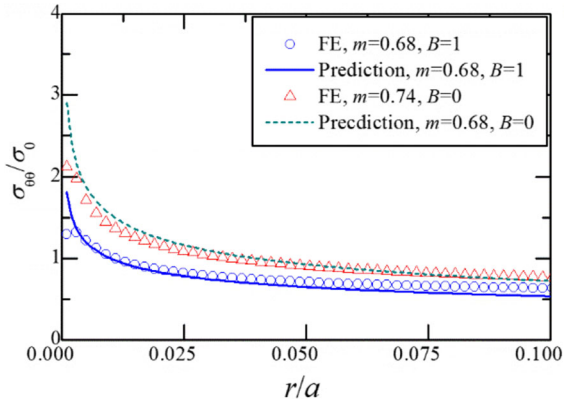


**Fig. 15** Verification of the predicted stress field

contribution of mode II case even under mode I conditions according to the investigations given by Ayatollahi and coworkers (2002, 2018), however, this effect is currently ignored in this paper.

## 5 Concluding remarks

With the theoretical and numerical investigations of this paper, the material constraint effect is discussed for a mismatch cracked weldment under biaxial loading. Through those studies, the answer to the question that "Can material constraint effect be characterized independently under creeping conditions based on rigorously higher order asymptotic solution?" is "Yes, but not that rigorous." In detail, the conclusions are drawn as following:

1) Under biaxial loading condition, the variations of the constraint effect for a crack tip in mismatch creeping solids are very different from that of homogeneous creeping solids. The total constraint level for crack tip under undermatch condition is higher than overmatch condition. Otherwise, the condition with positive biaxiality could lead to a higher constraint level compared with the condition under negative biaxiality.
2) Although the total constraint level has been divided into the so called geometry constraint effect and material constraint effect in this paper, the effect of loading biaxiality, crack depth and material mismatch contribute as a whole to the entire constraint level. They could

not be separated independently from rigorously asymptotic solutions for those cases with positive biaxiality as they can be influenced interactively.

3) For a crack tip field under non-positive biaxiality, the material constraint effect can be characterized independently with some approximations. For these conditions, the material constraint effect characterized by $A^*_{2\mathrm{II}}$ and geometry constraint effected characterized by $A^*_{2\mathrm{I}}$ are approximately independent on material mismatch factor and crack depth ratio as well as stress biaxiality, respectively.
4) An empirical formula has been presented to characterize the geometry constraint effect $A^*_{2\mathrm{I}}$ and material constraint effect $A^*_{2\mathrm{II}}$, in which the geometry constraint is a function of crack depth and loading biaxiality, and material constraint effect is a function of mismatch factor.

It should be noted that the extension of the work presented in this paper to a more general mismatch weldment, which contains more mismatching material properties, is also valuable in future work.

**Acknowledgements** Yanwei Dai acknowledges the support from the National Natural Science Foundation of China (11902009), the Beijing Municipal Natural Science Foundation (2204074), and the Scientific Research Common Program of Beijing Municipal Commission of Education (KM202010005034). The authors thank Prof. Yuh-Jin Chao for useful suggestions on improving the paper. The authors also would like to thank Hui Peng for his assistance in the computation and data collection of this paper.

## References

Alang NA, Nikbin K (2018) An analytical and numerical approach to multiscale ductility constraint based model to predict uniaxial/multiaxial creep rupture and cracking rates". Int J Mech Sci 135:342–352

Alves DN, Almeida JG, Rodrigues MC (2020) Experimental and numerical investigation of crack growth behavior in a dissimilar welded joint. Theor Appl Fract Mech 109:102697

Ayatollahi MR, Berto F (2018) Evolution of crack tip constraint in a mode II elastic-plastic crack problem. Phys Mesomech 21:173–177

Ayatollahi MR, Smith D, Pavier M (2002) Crack-tip constraint in mode II deformation. Int J Fract 113:153–173

Budden PJ, Ainsworth RA (1999) The effect of constraint on creep fracture assessments. Int J Fract 97(1):237–247

Burstow MC, Ainsworth RA (1995) Comparison of analytical, numerical and experimental solutions to problems of deeply cracked welded joints in bending. Fatigue Fract Eng Mater Struct 18:221–234

Burstow MC, Howard IC, Ainsworth RA (1998) The influence of constraint on crack tip stress fields in strength mismatched welded joints. J Mech Phys Solids 46(5):845–872

Chao Y, Zhang L (1997) Tables of plane strain crack tip fields: HRR and higher order terms. University of South Carolina, Columbia, pp 97–101

Chao YJ, Zhu XK (2001) Zhang L (2001) Higher-order asymptotic crack-tip fields in a power-law creeping material. Int J Solids Struct 38:3853–3875

Cui P, Guo WL (2020) Crack-tip-opening-displacement-based description of creep crack border fields in specimens with different geometries and thicknesses. Int J Solids Struct 188–189:37–55

Dai YW, Liu DH, Liu YH (2016) Mismatch constraint effect of creep crack with modified boundary layer moel. J Appl Mech 83(3):031008

Dai YW, Liu YH, Chao YuhJ (2017) Higher order asymptotic analysis of crack tip fields under mode II creeping conditions. Int J Solids Struct 125:89–107

Dai YW, Liu YH, Qin F, Chao YuhJ, Berto F (2019) Estimation of stress field for sharp V-notch in power-law creeping solids: an asymptotic viewpoint. Int J Solids Struct 2019:189–204

Dai YW, Liu YH, Qin F, Chao YJ, Chen HF (2020a) Constraint modified time dependent failure assessment diagram (TDFAD) based on C(t)-$A_2$(t) theory for creep crack. Int J Mech Sci 165:105193

Dai Y, Qin F, Liu YH, Feng WZ, Qian GA (2020b) Estimation of $C_*$-integral for central cracked plate under biaxial loading. Int J Appl Mech 12(7):2050079

Dai YW, Qin F, Liu YH, Chao YJ (2021) On the second order term asymptotic solution for sharp V-notch tip field in elasto-viscoplastic solids. Int J Solids Struct 217–218:106–122

Duan C, Zhang S (2020) Two-parameter J-A estimation for weld centerline cracks of welded SE(T) specimen under tensile loading. Theor Appl Fract Mech 107:102435

Fan K, Wang GZ, Xuan FZ, Tu ST (2016) Correlation of material constraint with fracture toughness of interface regions in a dissimilar metal welded joint. Fatigue Fract Eng Mater Struct 39(10):1251–1262

Guo W, Chen Z, She C (2018) (2018) Universal characterization of three-dimensional creeping crack-front stress fields. Int J Solids Struct 152–153:104–117

Han JJ, Kim YJ, Jerng D, Nikbin K, Dean D (2015) Quantification of creep stresses within HAZ in welded branch junctions. Fatigue Fract Eng Mater Struct 38:113–124

Hemer A, Milovic L, Grbovic A, Aleksic B, Aleksic V (2020) Numerical determination and experimental validation of the fracture toughness of welded joints. Eng Fail Anal 107:104220

Henry BS, Luxmoore AR (1997) The stress triaxiality constraint and the Q-value as a ductile fracture parameter. Eng Fract Mech 57(4):375–390

Jiang W, Yun L, Baozhu Z, Li SH, Xie XF, Shan-Tung T (2020) Characterization of creep constraint effect for brazed joint

specimens at crack tip by new constraint parameter as. Theor Appl Fract Mech 109:102707
Kumar S, Khan IA, Bhasin V, Singh RK (2014) Characterization of crack tip stresses in plane-strain fracture specimens having weld center crack. Int J Solids Struct 51:1464–1474
Kulkarni A, Dwivedi DK, Vasudevan M (2020) Microstructure and mechanical properties of A-TIG welded AISI 316L SS-Alloy 800 dissimilar metal joint. Mater Sci Eng 790:139685
Krishnan SA, Sarmah A, Moitra A, Sasikala G, Rao CL, Albert SK (2018) Study of fracture resistance of a weldment with a propagating crack. Int J Press Vessels Pip 168:210–218
Landes JBD, Begley JA (1976) A fracture mechanics approach to creep crack growth. ASTM STP 590:128–148
Lei Y (2004) J-integral and limit load analysis of semi-elliptical surface cracks in plates under combined tension and bending. Int J Press Vessels Pip 81:43–56
Ma HS, Wang GZ, Tu ST, Xuan FZ (2016) Unified correlation of geometry and material constraints with creep crack growth rate of welded joints. Eng Fract Mech 163:220–235
Nguyen BN, Onck P, van der Giessen E (2000) On higher-order crack-tip fields in creeping solids. J Appl Mech 67(2):372–382
Nikbin K (2004) Justification for meso-scale modelling in quantifying constraint during creep crack growth. Mater Sci Eng 365(1):107–113
O'Dowd N, Kolednik O, Naumenko V (1999) Elastic-plastic analysis of biaxially loaded center cracked plates. Int J Solids Struct 36:5639–5661
Ren XB, Zhang ZL, Nyhus B (2009) Effect of residual stresses on the crack-tip constraint in a modified boundary layer model. Int J Solids Struct 46(13):2629–2641
Riedel H (1990) Creep crack growth under small-scale creep conditions. Int J Fract 42:173–188
Saber M, Sun W, Hyde TH (2016) Numerical study of the effects of crack location on creep crack growth in weldment. Eng Fract Mech 154:72–82
Sharifi MH, Kaveh M, Saeidi Googarchin H (2018) Engineering critical assessments of marine pipelies with 3D surface cracks considering weld mismatch. J Solid Mech 10(2):354–363
Shlyannikov VN, Ilchenko BV, Boychenko NV (2009) Biaxial loading effect on higher-order crack tip parameters. In: Neu R, Wallin K, Thompson S (eds) Seventh international ASTM/ESIS symposium on fatigue and fracture mechanics (36th ASTM National Symposium on Fatigue and Fracture Mechanics). ASTM International, West Conshohocken, pp 609–640
Shlyannikov VN, Tumanov AV (2011) An inclined surface crack subject to biaxial loading. Int J Solids Struct 48(11–12):1778–1790
Shlyannikov VN, Tumanov AV, Zakharov AP (2014) The mixed mode crack growth rate in cruciform specimens subject to biaxial loading. Theor Appl Fract Mech 73:68–81
Tan JP, Wang GZ, Tu ST (2014) Xuan FZ (2014) Load-independent creep constraint parameter and its application. Eng Fract Mech 116:41–57
Velu M (2018) A short review on fracture and fatigue crack growth in welded joints. Mater Today 5(5):11364–11370
Wang X (2012) Two-parameter characterization of elastic–plastic crack front fields: surface cracked plates under uniaxial and biaxial bending. Eng Fract Mech 96:122–146
Wang G, Liu X, Xuan FZ, Tu ST (2010) Effect of constraint induced by crack depth on creep crack-tip stress field in CT specimens. Int J Solids Struct 47:51–57
Wang Z, Zhang YQ, Lam P-S, Chao YJ (2014) Creep analysis and constraint effect in a center-cracked plate under biaxial loading. ASME 2014 Pressure Vessels and Piping Conference: American Society of Mechanical Engineers V06ATA016-V06AT06A
Wang Y, Kannan R, Li L (2020) Insight into type IV cracking in Grade 91 steel weldments. Mater Design 190:108570
Wang Y, Zhang W, Huang H, Wang Y, Zhong W, Chen J, Feng Z (2021) Clarification of creep deformation mechanism in heat-affected zone of 9Cr steels with In Situ experiments. Scripta Mater 194:113640
Wu D, Jing H, Lianyong X (2020) Engineering application of enhanced C*-Q* two parameter approaches for predicting creep crack initiation times. Eur J Mech A-Solids 82:104013
Xu L, Zhao L, Han Y, Jing H, Gao Z (2017a) Characterizing crack growth behavior and damage evolution in P92 steel under creep-fatigue conditions. Int J Mech Sci 134:63–74
Xu L, Zhao L, Jing H, Han Y (2017b) Evaluation of multiple cracks interaction effect subjected to biaxial tension under creep regime. Int J Mech Sci 122:203–214
Xuan FZ, Tu ST, Wang Z (2004) $C^*$ estimation for cracks in mismatched welds and finite element validation. Int J Fract 126:267–280
Yang B, Xuan FZ (2018) Creep behavior of subzones in a CrMoV weldment characterized by the in-situ creep test with miniature specimens. Mater Sci Eng 723:148–156
Zhang Z, Hauge M, Thaulow C (1996) Two-parameter characterization of the near-tip stress fields for a bi-material elastic-plastic interface crack. Int J Fract 79:65–83
Zhang Z, Thaulow C, Hauge M (1997) Effects of crack size and weld metal mismatch on the has cleavage toughness of wide plates. Eng Fract Mech 57:653–664
Zhang Y, Shuai J, Lv Z, Xu K (2020) Investigation of the effects of material parameters on the relationship between crack tip constraint and CTOD fracture toughness. Theor Appl Fract Mech 108:102615
Zhou H, Biglari F, Davies CM, Mehmanparast A, Nikbin KM (2014) Evaluation of fracture mechanics parameters for a range of weldment geometries with different mismatch ratios. Eng Fract Mech 124:30–51